High-Throughput Production With Improved Functionality and Graphitization of Carbon Fine Fibers Developed from Sodium Chloride-Polyacrylonitrile Precursors

Mandana Akia,[1] **Lee Cremar**,[1] **Manuel Seas**,[2] **Jahaziel Villarreal**,[1] **Alejandra Valdez**,[1] **Mataz Alcoutlabi**,[1] **Karen Lozano**[1]
[1]*Department of Mechanical Engineering, University of Texas Rio Grande Valley, Edinburg, Texas 78539*
[2]*School of Biomedical Engineering, Science, and Health Sciences, Drexel University, Philadelphia, Pennsylvania*

Fine polyacrylonitrile (PAN) fibers were produced through a scalable centrifugal spinning process. Sodium chloride (NaCl) was added to the PAN-dimethylformamide solution to decrease the surface tension and consequently promote a decrease in fiber diameter while increasing the fiber output. The fiber preparation process involved the centrifugal spinning of the PAN-based solution; developed fibers were stabilized in air at 240°C followed by carbonization at 800°C under a Nitrogen atmosphere. The addition of sodium chloride to the PAN solution led to a 37% decrease in the carbon fiber diameter. The carbon fibers were analyzed by scanning electron microcopy, transmission electron microscopy (TEM), X-ray diffraction, X-ray photoelectron spectroscopy (XPS) and electrochemical experiments. The TEM results revealed improved graphitization with the addition of sodium chloride. The XPS analysis showed increased functionality (e.g. O_2) on the surface of carbon fibers obtained from PAN/NaCl precursor fibers. A significant improvement was achieved in the electrochemical performance of carbon fibers made from PAN/NaCl precursor fibers compared to those made from pure PAN precursor fibers. POLYM. ENG. SCI., 58:2047–2054, 2018. © 2018 Society of Plastics Engineers

INTRODUCTION

The interest in the production of carbon fibers has remained active because of their attractive electrical and thermo-physical properties and therefore, a myriad of potential applications [1, 2]. Carbon fibers can exhibit relatively high electrical conductivity, high mechanical strength, high thermal stability, and are known to be lightweight compared to other structures [1, 3–7]. The morphology and structure of carbon fibers can also be tailored to possess high specific surface area ($> 3000\ m^2\ g^{-1}$) and super hydrophobicity (c.a. $\sim 130°$) [8, 9]. The production of fine fibers (nano to single digit micron scale) can be achieved through a variety of methods, such as: wet chemistry methods, solution/melt blowing, and spinning methods (wet, dry, and melt spinning) [10–12].

Drawing and electrospinning (ES) are the most used spinning methods to produce polymer and polymer composite fibers [13, 14]. The diameter of fibers produced by ES can range from tens of nanometers to a few micrometers, however, at the lab scale, the fiber production rate is low, from 0.01 to 1.0 grams per hour depending on the flow rate, polymer concentration and voltage used. Unlike the ES method, the Forcespinning (FS) method, which applies centrifugal force to a polymer solution or melt, produces fibers in the absence of an electric field, therefore broadening the choice of materials to be spun into fine fibers. FS can produce highly homogeneous fibers with diameters that can range from tens of nanometers to several microns depending on the selected processing parameters and solution/melt properties [15, 16].

Carbonaceous materials have been widely used in electrochemical capacitors and energy storage devices such as supercapacitors and as electrodes in Lithium-ion batteries (LIBs) [17–20]. These devices are ideal for use in portable electronics, hybrid electric vehicles, and industrial power management, where high energy density, high specific power, and longer cycle life are required [21, 22]. Results reported in the literature show that the Li-intercalation and deintercalation (between Li and carbon) depends substantially on the crystalline phase, microstructure, and morphology of the carbonaceous materials [23, 24]. The pseudo-capacitive characteristics of the carbon-based materials, which occurs via redox reactions or faradic charge transfer reactions between the electrode and ions in the electrolyte, are brought about by surface modifications or doping with heteroatoms/functional groups such as: O, N, B, P, etc. [22].

In this study, the development of carbon fibers from PAN and PAN/NaCl precursor solutions is presented with preliminary data on the potential use of these fibrous mats as anode materials for LIBs. The effect of sodium chloride on the production rate, graphitization of fine PAN fibers and on the electrochemical performance of the carbon fiber anodes is systematically investigated.

MATERIALS AND METHODS

Materials

PAN (polyacrylonitrile) with molecular weight of 150,000 was used as the polymer precursor. The selected solvent was N-dimethylformamide (DMF). Sodium chloride was added to the PAN-DMF solution. All materials were purchased from Sigma Aldrich, USA.

Production of Carbon Fibers

A solution containing 11 wt% of PAN was prepared using DMF as the solvent. Sodium chloride was added to the PAN solution at different weight percentages (0–10 wt% of NaCl): 0

Correspondence to: K. Lozano; e-mail: Karen.Lozano@UTRGV.edu
Contract grant sponsor: National Science Foundation under PREM grant DMR; contract grant number: 1523577; contract grant: National Institute on Minority Health and Health Disparities of the National Institutes of Health; contract award number: G12MD007591.
DOI 10.1002/pen.24816
Published online in Wiley Online Library (wileyonlinelibrary.com).
© 2018 Society of Plastics Engineers

FIG. 1. Schematic of the input and output process for PAN-based carbon fiber production using the Forcespinning (FS) technique. [Color figure can be viewed at wileyonlinelibrary.com]

wt% (P-1), 5 wt% (P-2), and 10 wt% (P-3). The prepared solutions were stirred at room temperature for 24 hours. A lab scale Cylone L-1000M (FibeRio Technology) was used to produce the PAN fibers from the prepared solutions. Two milliliters of the homogenous PAN/NaCl solution were injected into a cylindrical spinneret with two 30 gauge (half inch) bevel needles attached at each end. The solutions were spun at angular velocities ranging from 7000 to 9000 rpm under an ambient relative humidity of 65%. The FS of PAN fibers was performed at room temperature. As shown in Fig. 1, the fibers were collected as nonwoven square mats. The obtained fibrous mats were stabilized in air at 240°C for 2 hours, and then carbonized under a nitrogen atmosphere at 800°C for 1 hour at a rate of 3°C min^{-1}.

Surface and Fiber Morphology Characterization

The surface morphology of the as-spun PAN fibers and carbon fibers was evaluated using Scanning Electron Microscopy (SEM), a Sigma VP Carl Zeiss, low voltage (1 kV) for the as-spun fibers and 7 kV for the carbonized fibers. Thermogravimetric analysis (TGA-DTG) was performed using a TA Instrument SDT Q600 TGA, with a ramping/heating rate of 10°C min^{-1} under a nitrogen atmosphere. Transmission Electron Microscopy (TEM) was conducted using a JEOL-2010 TEM, operated under a high voltage (200 kV). X-ray diffraction (XRD) patterns for the PAN and carbon fibers were obtained using a Bruker D8 Advanced X-ray Diffractometer with a range of $2\theta = 10$–90° at a scan rate of 1°C min^{-1}. X-ray photoelectron spectrometry (XPS) was used to evaluate the surface morphology of carbon fibers using a Thermoscientific K-α XPS equipped with a micro-focused monochromated Al K-α X-ray source, with 1eV for scans and 1 keV for depth analysis. The electrochemical performance of the carbon fiber anodes was evaluated using coin cells of CR2032 type (Henergy Corp) and assembled in a glovebox (Maubran) filled with pure argon gas and oxygen and moisture content <0.5 ppm. Lithium metal foil (Henergy Corp) was used as the counter electrode while glass fibers membranes were used as the separator. The electrolyte used was 1 M lithium hexafluorophosphate ($LiPF_6$), dissolved in 1/1 (V/V) ethylene carbonate (EC)/ethyl methyl carbonate (EMC) (MTI Corp.). Charge (lithium insertion) and discharge (lithium extraction) galvanostatic experiments were conducted using a Land automatic battery cycler at a current density of 100 mA g^{-1} between cutoff potentials of 0.05 and 3.00 V.

RESULTS AND DISCUSSION

SEM and TGA/DTG Analysis of the as-Prepared Fibers

Figure 2 shows the SEM micrographs of the as-spun PAN fibers (sample P-1 [0 wt% of NaCl] and sample P-2 [5 wt% of NaCl]). These SEM images show long, continuous fibers with a porous surface for sample P-1 (Fig. 2a). In the case of sample P-2, a highly heterogeneous surface is observed; the fibers have a porous surface with the presence of protruding salt crystals (Fig. 2b). The throughput of the fibers made from PAN/NaCl solutions (samples P-2 and P-3) increased by 7–8%. Additionally, collection of the PAN/NaCl fibers was facilitated when compared to the pure PAN fibers. Figure 2c shows the thermogravimetric analysis of the samples P-1, P-2, and P-3 with their respective derivative weight profiles (DTG). The DTG curves show three steps in the degradation process of all the samples. The first weight loss is attributed to the removal of water moisture and solvent residues and starts at around 100°C. The second degradation is observed at ~285°C for sample P-1 and ~275°C for samples P-2 and P-3 (with the highest weight loss), while the third degradation step is detected at ~425°C for all the samples which corresponds to the PAN degradation. The weight loss for all samples stabilizes at approximately 550°C, which indicates the carbonization temperature of PAN-based fibers. A total weight loss of 63% was observed for the pure PAN fibers, which is higher than that for the samples P-2 and P-3, 62% and 59%, respectively.

SEM and TEM Analyses of the Carbon Fibers

Figure 3a shows the SEM images of the carbonized PAN fibers (sample P-1). The average diameter of these fibers was found to be 1050 nanometers (nm), as depicted in Fig. 3e. The SEM images for sample P-2 and the fiber diameter distribution (histogram) are shown in Fig. 3b and f, respectively, which indicate a significant decrease of 37% in fiber diameter compared to that for sample P-1. The upper inset in Fig. 3b shows the decorated carbon fibers. The SEM images for sample P-3 (10 wt% NaCl) is shown in Fig. 3c. As shown in the histogram displayed in Fig. 3g, the average fiber diameter for this sample is 740 nm. The addition of NaCl to the PAN solution promoted a decrease in surface tension which led to smaller fiber diameters with a significant decrease in bead formation (Fig. 3d) [25]. As the solution jet is stretched, the lower surface tension of the polymer solution allows for higher elongation during the centrifugal spinning process. In the case of the 10 wt% NaCl sample, it is

 DOI 10.1002/pen

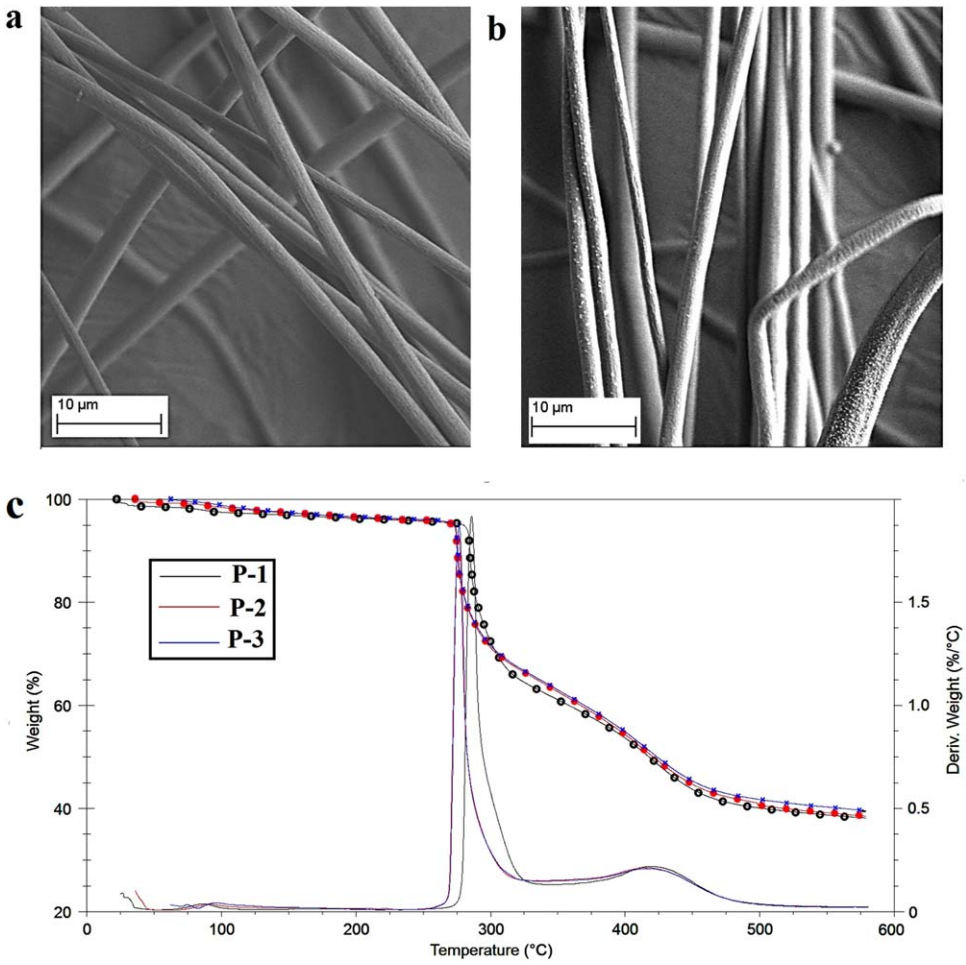

FIG. 2. SEM micrographs of (a) sample P-1 (as-prepared PAN-based fibers) and (b) sample P-2 with 5 wt% of NaCl, (c) TGA- DTG curves for samples P-1, P-2, and P-3. [Color figure can be viewed at wileyonlinelibrary.com]

observed that the critical concentration has been exceeded and the fiber diameter increased.

Figure 4 shows the TEM and HRTEM images for samples P-1 (pure PAN) and P-2 (with 5 wt% of NaCl). The TEM analysis indicated an ordered graphitic structure in sample P-2 (Fig. 4b) as compared to the pure PAN-based carbon fibers (Fig. 4a). The high-resolution images for sample P-2 display the graphite layers with a spacing measuring ~0.33 nm (Fig. 4c and d). The cross-sectional image shows a well-defined graphite structure as indicated by the aligned parallel layers/lines, which are represented by the dark and bright areas.

XPS Analysis

Figure 5a–e shows the X-ray photoelectron spectroscopy analysis for all the carbonized PAN fibers. All the samples show a peak at 284.5 eV which corresponds to the C1s graphitic peak found in carbon materials [26, 27]. The O1s oxygen peak appears at a range between 528–536 eV. The N1s peak at 397 eV is related to the bonding of carbon to nitrogen, which occurred during the carbonization process of PAN fibers at 800°C. For samples, P-1 and P-2, the peak observed at 1070 eV is attributed to Na1s, and accompanied by the Na Auger peak at 496 eV. Figure 5b displays the depth profile analysis of oxygen functional groups where a significant increase of oxygen percentage for samples P-2 and P-3 is observed. This is consistent with the XPS results reported by Singhal *et al.*, where the incorporation of NaCl into PAN followed by carbonization facilitated an increase in the oxygen content [27]. Figure 5c–e shows the fitted spectra for the C1s peak assigned to the graphitic carbon present in all samples. Sample P-1 depicts two more peaks at 288.2 and 290.7 eV corresponding to the C═O group and π–π^* transition band. Sample P-2 displays a peak at 288.2 eV with higher intensity when compared to sample P-1. For sample P-3, a peak at 289.8 eV related to O─C═O functional group is observed indicating that this sample possess more oxygen containing functional groups when compared to other samples.

Table 1 shows the atomic composition of samples P-1, P-2, and P-3, based on the XPS analysis. The oxygen atomic percentage and oxygen-to-carbon ratio is higher on the surface of the fibers (depth profile analysis) than that in the core of carbon fibers. A comparison between the surface composition of nitrogen and nitrogen-to-carbon ratio in different samples reveals a slightly decrease in nitrogen percentage with an increase in salt content. However, the bulk analysis showed a little increase in the nitrogen percentage. As illustrated in Table 1, the chloride is completely removed after the carbonization step for samples P-2 and P-3.

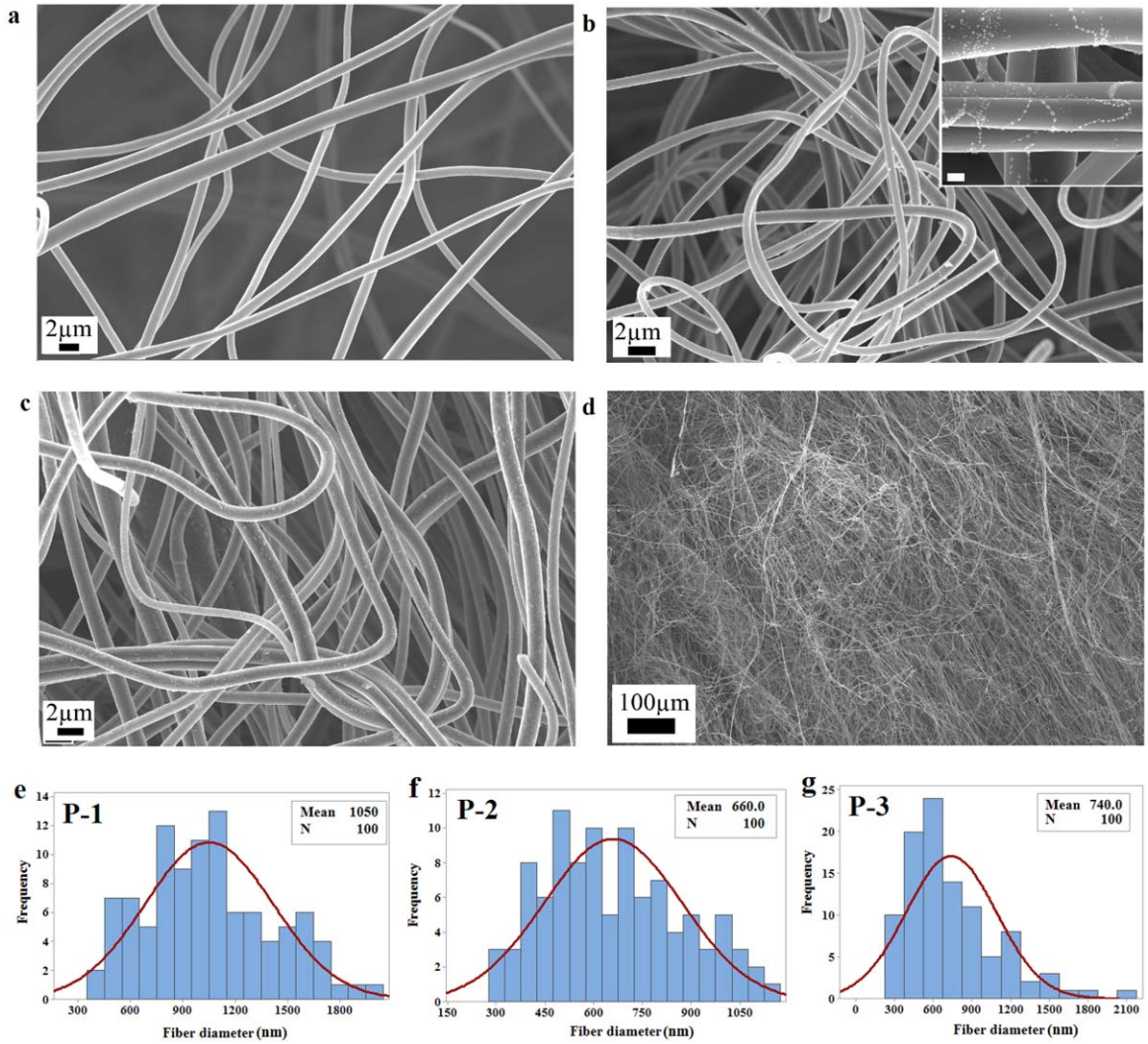

FIG. 3. SEM images of (a) carbonized fibers without additive, (b) with 5 wt% of NaCl—the scale bar for upper inset is 300 nm, and (c) with 10 wt% of NaCl. (d) A micrograph image of the mat showing homogeneous fiber formation without beads for sample P-2. Histograms of fiber diameters for the samples P-1, P-2, and P-3, respectively (e, f, and g). [Color figure can be viewed at wileyonlinelibrary.com]

XRD Analysis

Figure 6 shows the XRD analysis for the carbonized PAN fibers where two main peaks with different intensities are observed in all samples. The spectra of sample P-1 shown in Figure 6 indicate that the peaks between $2\theta = 15$–$30°$ are related to the (002) lattice plane of graphite in carbon fibers [28, 29] while the peak appearing between $2\theta = 40$–$50°$ corresponds to the X-ray reflections of the (100) crystallographic lattice plane. The broad high-intensity peaks at 24.5° and low-intensity peaks at 43.5°, observed for samples P-2 and P-3, are assigned to (002) and (100) planes, respectively. A comparison between the peaks for different salt concentrations revealed the higher peak intensities for sample P-2 compared to sample P-3; this related to the higher graphitization structures of sample P-2, as confirmed by the HRTEM results. The XRD spectra shown in Fig. 6 clearly indicate the absence of peaks for sodium chloride crystals. The carbonization step of PAN fibers led to the complete removal of chloride (as confirmed by the XPS analysis) without requiring postprocessing removal steps. Results reported in the literature showed that sodium chloride crystals can be removed from carbon fibers by using acid bath-based treatments after carbonization [27].

Electrochemical Performance of Carbon Fiber Anodes

Figure 7 shows the charge/discharge curves and Coulombic efficiency of carbon fiber anodes (samples P-1, P-2, and P-3) at a constant current density of 100 mA g^{-1} over a potential window of 0.05–3 V. Figure 7a shows that the voltage steeply declines to about 0.3–0.4 V during the first discharge process (lithium insertion), and then slowly decreases until a total discharge capacity of 407 mAh g^{-1} is reached. This capacity value, which is higher than the theoretical capacity of graphite, can be partially assigned to the discharge storage of carbon fibers via the intercalation mechanism of C with Li+. The plateau at 0.3–0.4 V may also be associated with the electrolyte

 DOI 10.1002/pen

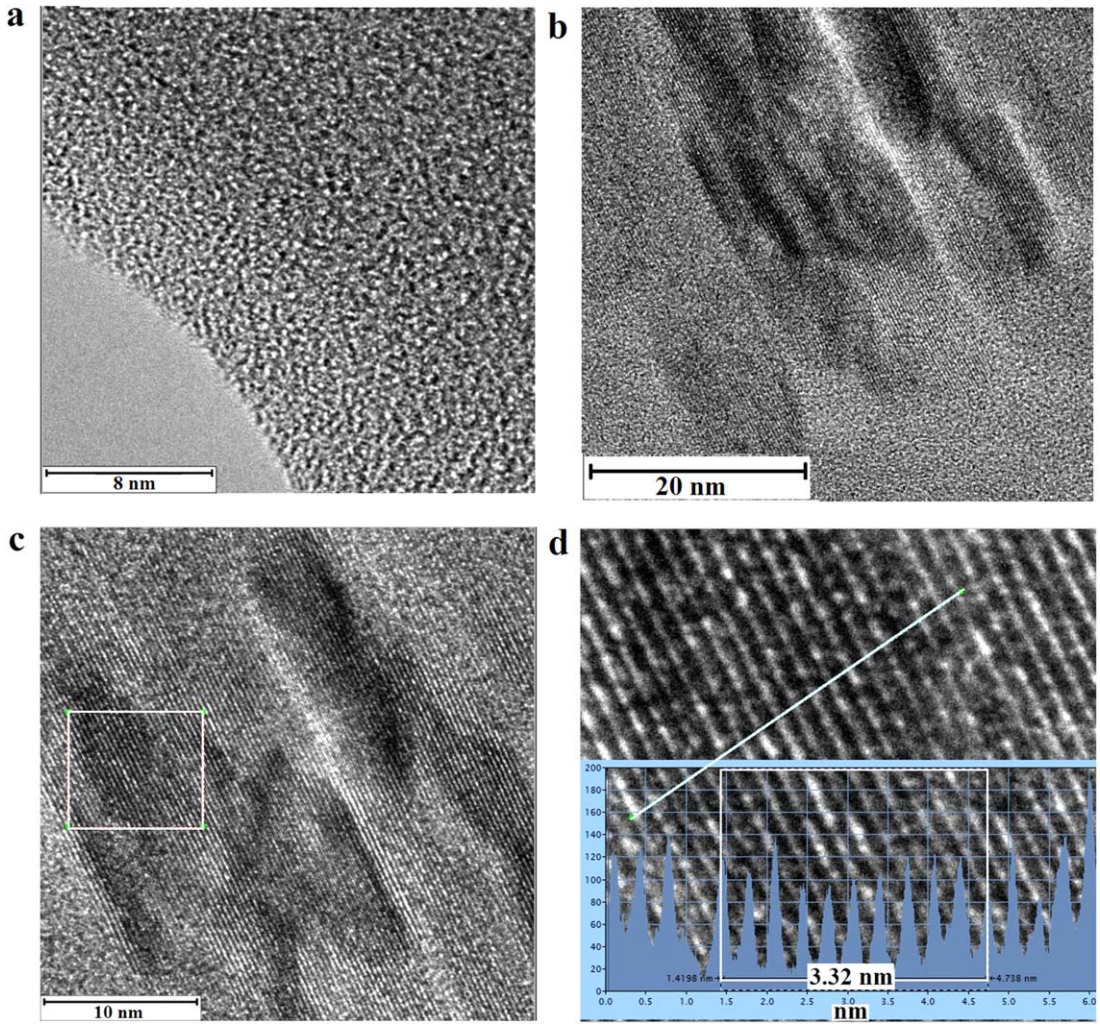

FIG. 4. TEM images for carbon fibers prepared from PAN solutions containing 0 and 5 wt% of NaCl. (a) TEM image of the pure carbon fiber, (b) TEM image of sample P-2 with 5 wt% of NaCl, (c) HRTEM image of sample P-2, showing the graphite structure, and (d) the intensity profile along the line perpendicular to the graphitic lines/plane shown in Fig. 4c. [Color figure can be viewed at wileyonlinelibrary.com]

decomposition and SEI formation [30]. The corresponding first-cycle discharge profiles show a slight polarization at around 0.75 V, followed by smoothly increasing curves, which show a slight polarization at around 0.25 V. The first-cycle charge capacity is about 140 mAh g^{-1}, corresponding to a Coulombic efficiency of about 34% (Fig. 7d). This relatively low Coulombic efficiency can be attributed to the decomposition of the electrolyte and the formation of an SEI film or the existence of other inactive materials in the carbon fiber anode. The high irreversible capacity at the first cycle (140 mAh g^{-1}) can be because of the large surface area of the carbon fibers and the slow kinetics of the inactive sites. However, after the first cycle, the value of the Coulombic efficiency remains nearly 100% (Fig. 7d). In addition, the value of the reversible capacity of carbon fibers (Fig. 7a) decreases with increasing cycles and reach a value of about 103 mAh g^{-1} after 100 charge/discharge cycles. The charge/discharge curves of the samples P-2 and P-3 are shown in Fig. 7b and c, the voltage plateau shows higher values (0.6–0.7 V) than those obtained for pure carbon fibers (0.3–0.4 V). During the first discharge process (lithium insertion), the total discharge capacity of 470 and 562 mAh g^{-1} were obtained for samples P-2 and P-3, respectively. These high capacity values can be partially assigned to the polymer surface-layer formation and the charge storage via surface charge-transfer mechanism [31, 32]. The charge capacity (Li-deinsertion) of the samples P-2 and P-3 at the first cycle are 200 and 232 mAh g^{-1}, respectively (Fig. 7b and c). These values are higher than that for pure carbon fibers (sample P-1) (Fig. 7a). After 75 cycles, the reversible capacity of sample P-2 remains relatively constant at around 136 mAh g^{-1}, while for the sample P-3 and after 50 cycles, the reversible capacity remains constant at 139 mAh g^{-1}. Based on results reported in the literature, electrode materials made from carbon- enriched with heteroatoms, e.g. oxygen [22, 33] and nitrogen groups [34] showed improved storage capability and cyclability of the battery as needed for applications requiring high energy density and long cycle life [35]. The improved cycling performance of the samples P-2 and P-3 can be ascribed to their improved functionality (incorporation of heteroatoms [oxygen]) and morphology (smaller fiber diameter) compared to sample P-1. The decrease in carbon fiber

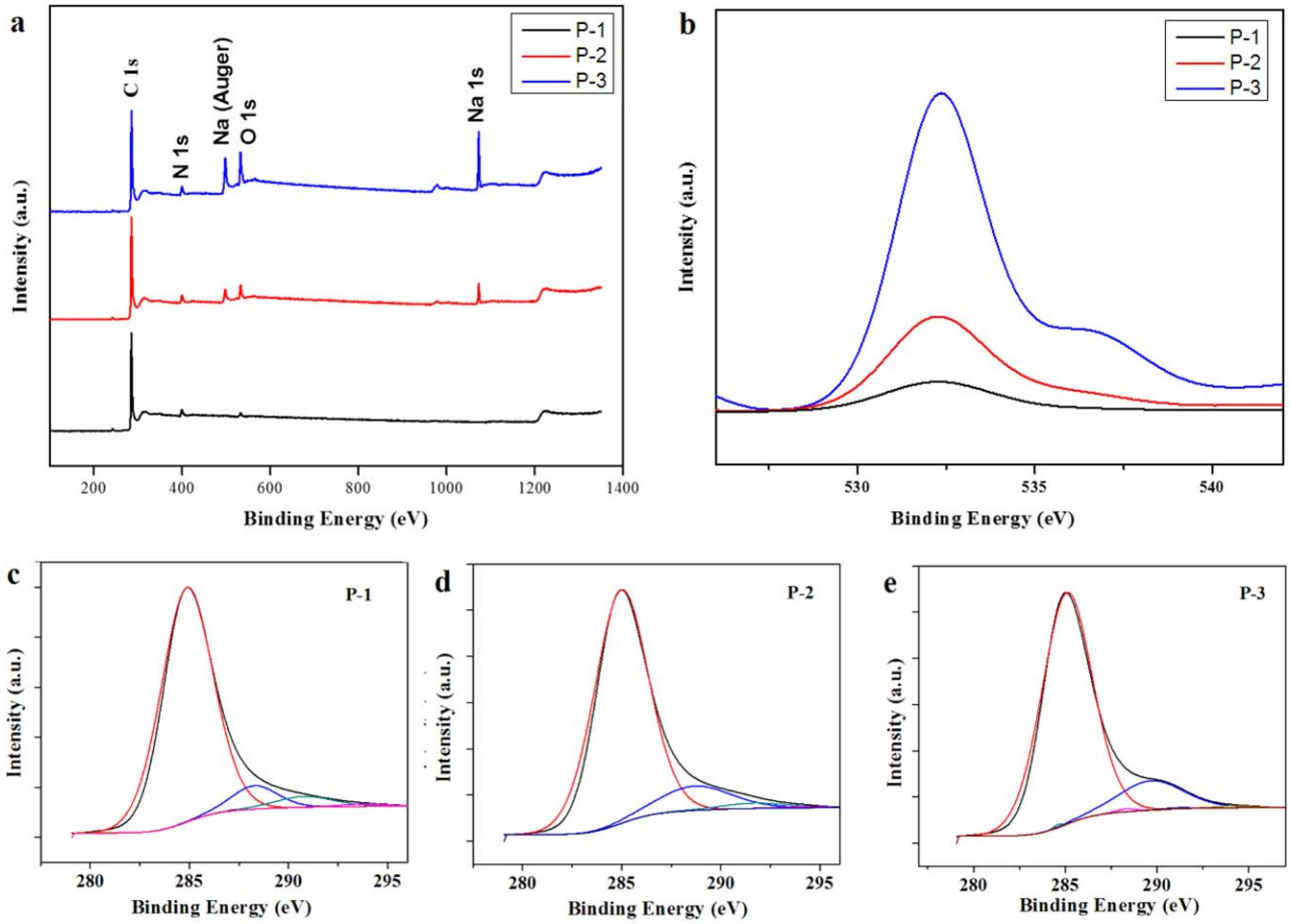

FIG. 5. (a) XPS survey spectra for carbonized PAN fibers (P-1), carbonized PAN fibers prepared from solutions containing 5 wt% (P-2), and 10 wt% (P-3) of sodium chloride, (b) A comparison of oxygen content based on the depth profile analysis and deconvolution of C1s XPS peak for all samples (c, d, and e). [Color figure can be viewed at wileyonlinelibrary.com]

diameter, because of the addition of NaCl to the PAN solution, (i.e. high surface area of carbon fibers compared to bulk graphite) resulted in faster Li-ion diffusion at the electrolyte–anode interface and shorter pathways for both Li ions and electrons, therefore, leading to higher discharge capacities for samples P-2 and P-3 compared to the sample P-1. Figure 7d shows that the values of the Coulombic efficiency for the samples P-2 and P-3 at the first cycle are 43% and 41%, respectively, and after the second cycle, the coulombic efficiency of these carbon fiber anodes is almost 100%.

Figure 8 shows the rate performance of the carbon fiber anode (sample P-2) at different current densities of 50, 100, 200, 400, and 500 mA g^{-1}. The rate performance of the carbon fibers is evaluated by increasing the current density stepwise from 50 to 500 mA g^{-1} every 10 cycles and going back stepwise to 50 mA g^{-1} after cycling at 500 mA g^{-1}. The results of Fig. 8 show that there is a loss in capacity at the first discharge cycle because of the formation of the SEI layer and the high surface area of the carbon fibers. These results are consistent with the cycle performance results of P-2 sample shown in Fig. 7d. As shown in Fig. 8, the first charge capacity of the carbon fibers at 50 mA g^{-1} is 306 mAh g^{-1} and after 10 cycles, the capacity reaches a value of 232 mAh g^{-1}. At a higher current density of 100 mA g^{-1}, the charge capacity remains constant at

TABLE 1. Surface and bulk atomic composition of samples P-1, P-2, and P-3.

Samples		Carbon	Oxygen	Nitrogen	Sodium	Oxygen/carbon (%)	Nitrogen/carbon (%)
P-1	Surface	87.0	5.22	7.7	0	6.00	8.85
	Depth (5 nm)	93.18	1.93	4.90	0	2.07	5.26
P-2	Surface	78.9	11.86	5.97	3.28	15.03	7.57
	Depth (5 nm)	85.76	5.87	5.25	3.12	6.45	6.12
P-3	Surface	73.3	15.75	5.24	5.7	21.49	7.15
	Depth (5 nm)	74.08	12.57	5.5	7.61	16.97	7.42

 DOI 10.1002/pen

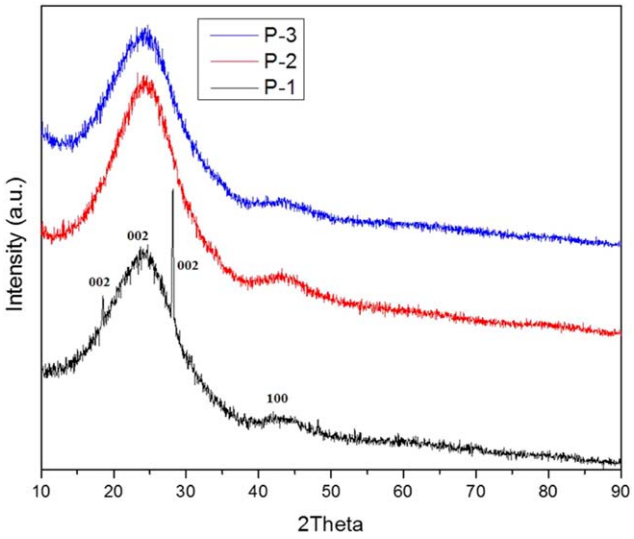

FIG. 6. XRD analysis of the carbonized PAN fibers with different weight percentages of NaCl (carbonized at 800°C). [Color figure can be viewed at wileyonlinelibrary.com]

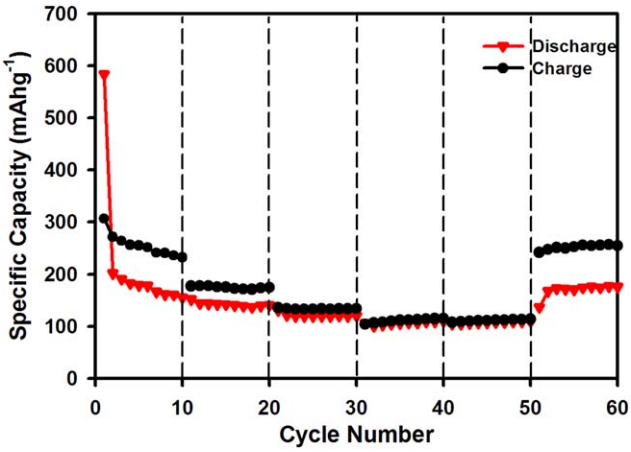

FIG. 8. The rate capability of the carbon fiber anode (sample P-2) at different current densities between 50 and 500 mA g^{-1}. [Color figure can be viewed at wileyonlinelibrary.com]

177 mAh g^{-1} and this is consistent with the results shown in Fig. 7b (sample P2). After charging the carbon fiber anode at the highest current density of 500 mA g^{-1}, the charge capacity reached a value of 113 mAh g^{-1} and when the carbon fiber anode was cycled back at 50 mA g^{-1}, the charge capacity was fully recovered to 255 mAh g^{-1} proving potential to be used as an electrode given the observed cycle performance and rate capability.

CONCLUSIONS

In this study, the effect of NaCl on the formation of PAN-based carbon fibers was investigated. The results of the average carbon fiber diameter revealed a 37% decrease in fiber diameter for samples prepared with 5 wt% of NaCl, compared to the pure

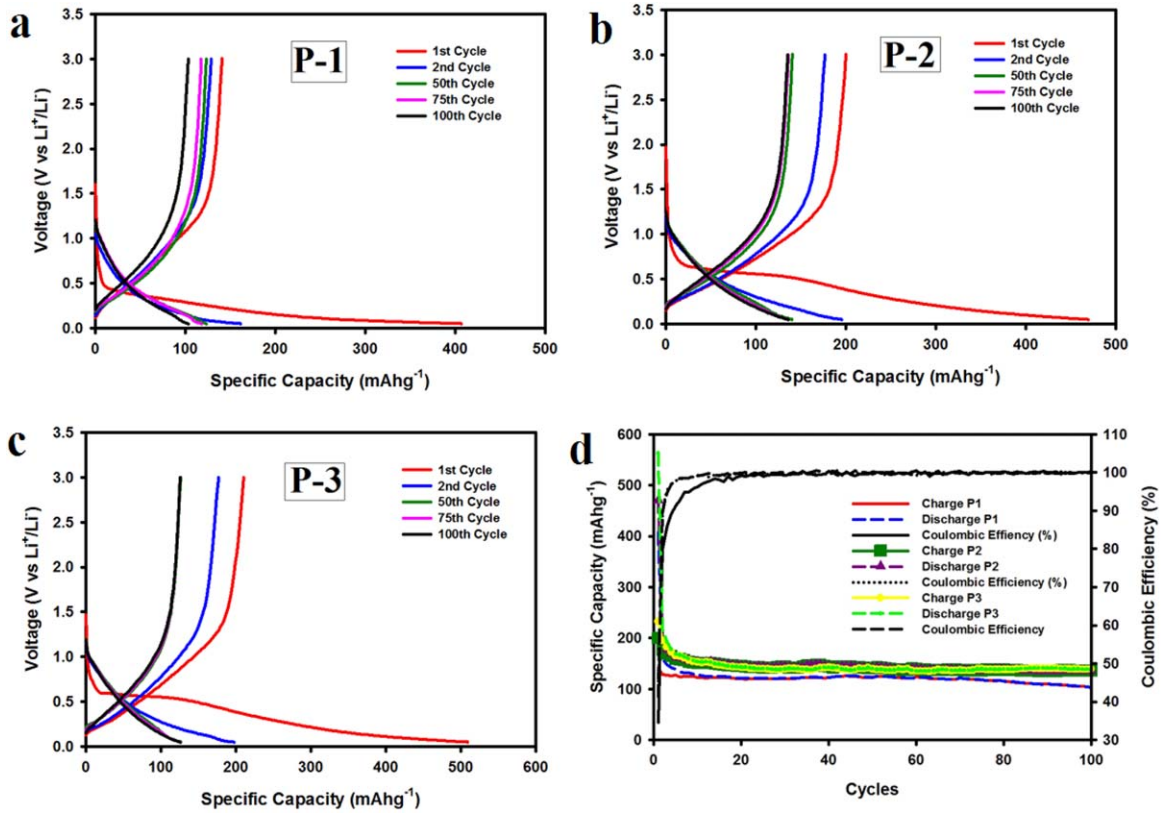

FIG. 7. Charge−discharge curves (a–c) and cycling performance (d) of carbon fibers made from PAN precursor fibers with weight percentages of sodium chloride, 0, 5, and 10 wt% (samples P-1, P-2, and P-3, respectively). [Color figure can be viewed at wileyonlinelibrary.com]

PAN fibers. Further increase in salt concentration (P3) led to a larger fiber diameter but still showed a 30% reduction when compared to sample P-1. The fiber throughput also increased at a range of 7–8% when compared to the pure PAN-based solution. The HRTEM results clearly revealed that the addition of salt to the PAN solution precursors resulted in graphitization improvement, which was depicted by the XRD results. Based on the XPS results, samples P-2 and P-3 showed increase in oxygen functional groups compared to the pure carbonized sample and complete removal of chloride after carbonization steps. The electrochemical performance results indicated an enhancement in the reversible capacity for the samples containing 5 and 10 wt% of sodium chloride, as a result of improved functionality and fiber morphology. The cycle performance results show stability and high potential cyclability for samples P-2 and P-3. Rate performance results for sample P-2 at different current densities confirm enhancing rate capability, which is consistent with cycle performance results.

ACKNOWLEDGMENTS

The authors gratefully acknowledge the Kleberg Advanced Microscopy Center of University of Texas at San Antonio (UTSA) for usage of the JEOL (2010) instrument.

REFERENCES

1. Z. Xu and C. Gao, *Mater. Today*, **18**, 480 (2015).
2. S. Liu, R. Liu, K. Han, H. Liu, and M. Yu, *Polym. Eng. Sci.*, **56**, 1313 (2016).
3. N. Behabtu, C.C. Young, D.E. Tsentalovich, O. Kleinerman, X. Wang, A.W.K. Ma, E.A. Bengio, R.F. ter Waarbeek, J.J. de Jong, R.E. Hoogerwerf, S.B. Fairchild, J.B. Ferguson, B. Maruyama, J. Kono, Y. Talmon, Y. Cohen, M.J. Otto, and M. Pasquali, *Science*, **339**, 182 (2013).
4. D. Choi, G.E. Blomgren, and P.N. Kumta, *Adv. Mater.*, **18**, 1178 (2006).
5. A.B. Dalton, S. Collins, E. Munoz, J.M. Razal, V.H. Ebron, J.P. Ferraris, J.N. Coleman, B.G. Kim, and R.H. Baughman, *Nature*, **423**, 703 (2003).
6. E. Frackowiak and F. Beguin, *Carbon*, **39**, 937 (2001).
7. M.E. Kozlov, R.C. Capps, W.M. Sampson, V.H. Ebron, J.P. Ferraris, and R.H. Baughman, *Adv. Mater.*, **17**, 614 (2005).
8. H.-Y. Hsiao, C.-M. Huang, M.-Y. Hsu, and H. Chen, *Sep. Purif. Technol.*, **82**, 19 (2011).
9. C.S. Sharma, A. Sharma, and M. Madou, *Langmuir*, **26**, 2218 (2010).
10. L. Feng, S. Li, H. Li, J. Zhai, Y. Song, L. Jiang, and D. Zhu, *Angew. Chem.*, **114**, 1269 (2002).
11. G. Liu, J. Ding, L. Qiao, A. Guo, B.P. Dymov, J.T. Gleeson, T. Hashimoto, and K. Saijo, *Chem. Eur. J.*, **5**, 2740 (1999).
12. C.R. Martin, *Chem. Mater.*, **8**, 1739 (1996).
13. A. Greiner, and J.H. Wendorff, *Angew. Chem. Int. Ed.*, **46**, 5670 (2007).
14. Z.-M. Huang, Y.-Z. Zhang, M. Kotaki, and S. Ramakrishna, *Compos. Sci. Technol.*, **63**, 2223 (2003).
15. K. Sarkar, C. Gomez, S. Zambrano, M. Ramirez, E. de Hoyos, H. Vasquez, and K. Lozano, *Mater. Today*, **13**, 12 (2010).
16. B. Weng, F. Xu, A. Salinas, and K. Lozano, *Carbon*, **75**, 217 (2014).
17. F. Cheng, Z. Tao, J. Liang, and J. Chen, *Chem. Mater.*, **20**, 667 (2008).
18. H. Zhou, S. Zhu, M. Hibino, I. Honma, and M. Ichihara, *Adv. Mater.*, **15**, 2107 (2003).
19. J.K. Lee, K.W. An, J.B. Ju, B.W. Cho, W.I. Cho, D. Park, and K.S. Yun, *Carbon*, **39**, 1299 (2001).
20. R. Chen, Y. Hu, Z. Shen, P. Pan, X. He, K. Wu, X. Zhang, and Z. Cheng, *J. Mater. Chem. A*, (2017).
21. J.R. Miller and P. Simon, *Sci. Mag.*, **321**, 651 (2008).
22. P. Simon and Y. Gogotsi, *Nat. Mater.*, **7**, 845 (2008).
23. J.R. Dahn, T. Zheng, Y. Liu, and J. Xue, *Science*, **270**, 590 (1995).
24. K. Sato, M. Noguchi, A. Demachi, N. Oki, and M. Endo, *Science*, **264**, 556 (1994).
25. G.O. Yahya, S.A. Ali, and E.Z. Hamad, *Polymer*, **37**, 1183 (1996).
26. Y. Geng, S.J. Wang, and J.-K. Kim, *J Colloid Interface Sci.*, **336**, 592 (2009).
27. R. Singhal and V. Kalra, *J. Mater. Chem. A*, **3**, 377 (2015).
28. Z. Zhou, C. Lai, L. Zhang, Y. Qian, H. Hou, D.H. Reneker, and H. Fong, *Polymer*, **50**, 2999 (2009).
29. E. Zussman, X. Chen, W. Ding, L. Calabri, D. Dikin, J. Quintana, and R. Ruoff, *Carbon*, **43**, 2175 (2005).
30. Y. Jiang, Z.-J. Jiang, L. Yang, S. Cheng, and M. Liu, *J. Mater. Chem. A*, **3**, 11847 (2015).
31. V.A. Agubra, L. Zuniga, D. Flores, J. Villareal, and M. Alcoutlabi, *Electrochim. Acta*, **192**, 529 (2016).
32. L. Ji, Z. Lin, M. Alcoutlabi, and X. Zhang, *Energy Environ. Sci.*, **4**, 2682 (2011).
33. E. Raymundo-Piñero, F. Leroux, and F. Béguin, *Adv. Mater.*, **18**, 1877 (2006).
34. S.L. Candelaria, B.B. Garcia, D. Liu, and G. Cao, *J. Mater. Chem.*, **22**, 9884 (2012).
35. D. Hulicova-Jurcakova, M. Kodama, S. Shiraishi, H. Hatori, Z.H. Zhu, and G.Q. Lu, *Adv. Funct. Mater.*, **19**, 1800 (2009).